Using comet plasma tails to study the solar wind

B. V. Jackson, A. Buffington, J. M. Clover, P. P. Hick, H. -S. Yu et al.

Citation: AIP Conf. Proc. **1539**, 364 (2013); doi: 10.1063/1.4811062
View online: http://dx.doi.org/10.1063/1.4811062
View Table of Contents: http://proceedings.aip.org/dbt/dbt.jsp?KEY=APCPCS&Volume=1539&Issue=1
Published by the AIP Publishing LLC.

Using Comet Plasma Tails to Study the Solar Wind

B. V. Jackson[a], A. Buffington[a], J. M. Clover[a], P. P. Hick[a], H. -S. Yu[a], and M. M. Bisi[b]

[a]*Center for Astrophysics and Space Sciences, University of California, San Diego, La Jolla, CA 92093, U.S.A.*

[b]*Institute of Mathematics and Physics, Aberystwyth University, Penglais Campus, Aberystwyth, SY23 3BZ, Wales, UK*

Abstract. The plasma tails of comets have been used as probes of the solar wind for many years, and well before direct solar wind measurements. Now, analyses utilizing the much greater regularity and extent of comet tails imaged from space detail outward solar wind flow much better than was previously possible. These analyses mark the location of the solar wind flow in three-dimensions over time much as do *in-situ* measurements. Data from comet plasma tails using coronagraphs and heliospheric white-light imagers provide a view closer to the Sun than where spacecraft have ventured to date. These views show that this flow is chaotic and highly variable, and not the benign regular outward motion of a quiescent plasma. While this is no surprise to those who study and characterize the solar wind *in situ* or use remotely-sensed interplanetary scintillation (IPS) techniques, these spacecraft images provide a visualization of this as never-before possible. Here we summarize the results of an analysis that determines solar wind velocity from multiple comet tails that were observed by the Solar Mass Ejection Imager (SMEI) and also by the inner Heliospheric Imager (HI) on board the Solar Terrestrial Relations Observatory Ahead (STEREO-A) spacecraft. Finally, we present results using a similar analysis that measures this same behavior using coronagraph observations in the low corona.

Keywords: Comets: interaction with solar wind; Solar wind; Turbulence: space plasma; Solar Corona: Coronal Mass Ejection
PACS: 96.50.Ek, 96.25.F-, 96.25.Fx; 96.60.Vg; 94.05.Lk; 96.60.P-; 96.60.ph

INTRODUCTION

Comet observations have long been used to infer the nature of the solar wind [1]. Classical techniques measure comet-tail aberration using ground-based comet images as described in Belton and Brandt [2]. In the first instance, comet tails revealed that the solar wind speed is supersonic [3]. The speed of the solar wind is related to the aberration angle (ε) of the comet plasma tail as shown in Figure 1a by [4]:

$$\tan\varepsilon = \frac{V \sin\gamma - w_{\varphi} \cos i'}{w_r - V \cos\gamma} \qquad (1)$$

where, respectively, V is the velocity of the comet; γ is the angle between the comet velocity and the antisolar direction; w_ϕ is the solar wind azimuthal component (measured positive in the sense of the solar rotation); i' is the inclination of the comet's orbit to the plane of the solar equator; and w_r is the solar wind radial component. Here ε is measured positive in the direction opposite the comet's velocity V. For typical solar wind speeds (~450 kms^{-1}) and $V \sin\gamma$ comet velocities (33 km s^{-1}) ε is about 5°. Measurements of comet photographs over the years yield ε values as displayed in Figure 1b. It is interesting to note that while an average value of ε is consistent with the nominal solar wind speed, this value has a great deal of variability as shown by the dashed anti-solar lines in Figure 1a, and also that retrograde values of ε predominate in the measurements. Brandt [4] interpreted this variability of ε to non-radial solar wind

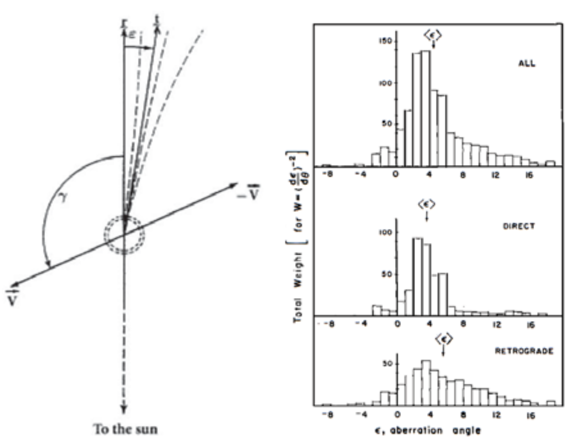

(a) (b)

FIGURE 1. a) Diagram showing the aberration of comet plasma tails as derived from the solar wind speed and comet motion. **b)** The distribution of aberration angles of type 1 comet tails (adapted from [4]).

Solar Wind 13
AIP Conf. Proc. 1539, 364-369 (2013); doi: 10.1063/1.4811062

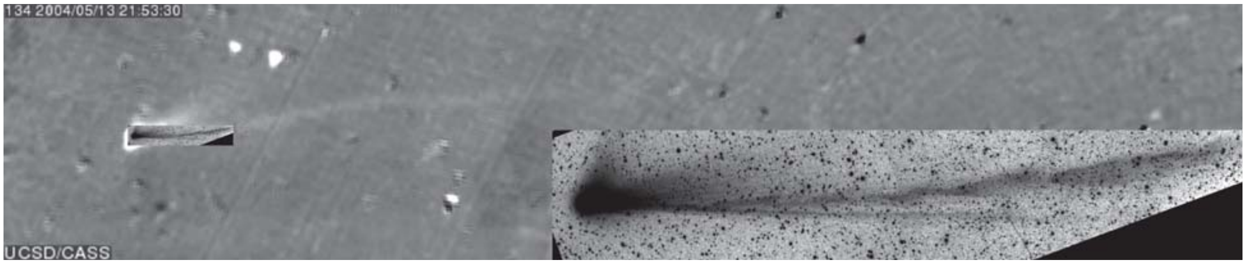

FIGURE 2. Composite diagram showing the comet C/2001 Q4 (NEAT) nucleus and tail viewed by ground based observers (inset of a typical 9° field of view lower right, and also placed upon the nucleus), and the much more extensive view of this same comet plasma tail in SMEI images (adapted from [21]).

motions or a structured comet nucleus or both, and the retrograde predominance of ε to an average non-radial solar wind flow that is predominantly prograde, or opposite to the outward direction of the Parker spiral. From direct solar wind measurements, however, a prograde solar wind dominance of this magnitude is not indicated *e.g.*, from *in-situ* measurements by the two *Helios* spacecraft [5]. In a later article, Brandt attempted to determine a comet tail velocity difference with ecliptic latitude over a sample period of 75 years but found a null result [6], at odds with known extensions to polar coronal hole velocity observations in the ecliptic at that time (for one of the first reviews, see [7]). From interplanetary scintillation (IPS) (*e.g.*, [8]) a slightly later article utilizing polar velocity measurements from the UCSD radio array system [9] confirmed previous measurements of a solar cycle variation for polar solar wind speeds. These observations were later verified by direct *in-situ* polar velocity measurements from *Ulysses* [10, 11, 12].

The advent of spaceborne remotely-sensed comet-tail observations has changed things considerably. New images from coronagraphs, primarily the Large Angle Spectroscopic COronagraphs (LASCO) [13], and the inner Heliospheric Imager (HI) [14] part of the Sun-Earth Connection Coronal and Heliospheric Investigation (SECCHI) [15, 16] Heliospheric Imager-1 (HI-1) on board the Solar TErrestrial RElations Observatory Ahead (STEREO-A) spacecraft [17, 18], and finally from the Solar Mass Ejection Imager (SMEI) [19, 20] are able to view simultaneously the respective brightness of both the solar wind along lines of sight near the comet as well as the comet plasma tail itself. Additionally, the depth of the view and the radial extent of comet tail plasma viewing has increased from ground based photographs that are taken on a haphazard basis and as weather permits, to near continuous sequences of views of comet plasma tails, for even small comets, over distances as great as 1 AU (see Figure 2). Comet observations give a precise location of the comet nucleus within the three-dimensional (3D) solar wind, without the need to model for line-of-sight (LOS) effects. This can be used to advantage to provide a precise location probe of the solar wind to compare with the 3D location derived by appropriate modeling. Here we review the 3D analyses of comet plasma tails that take advantage of these spacecraft remote-sensing observations, and examine their ramifications for solar wind physics.

In the analyses used here we employ data from SMEI and the STEREO HI-1A instruments to measure the solar wind speed by tracking the propagation of the plasma tails of comets [22, 23]. The next section reviews measurements of the solar wind from comet plasma tails that show the wind to be structured and highly variable. Results indicate that the plasma visible a great distance (>10^6 km) from the nucleus of the comet has become entrained in the solar wind, and has little to do with the physics of the comet nucleus where the plasma tail originated. Moreover, we conclude that the "kinks" visible in these tails extending over great angular distances are frequently caused by varying solar wind speed at the location of the comet nucleus and that these manifest themselves as irregularities in the plasma tail as the comet plasma propagates radially outward.

Although this solar wind speed variability is no surprise to those who study the solar wind *in situ* or use remote-sensed IPS techniques, we show that the images of comet plasma tails provide a visualization of this variability as never-before possible, and enable a precise study of these effects in regions of the heliosphere not yet accessed by spacecraft *in-situ* measurements. We also show that a similar variability is indicated in very recent coronagraph analyses much closer to the solar surface.

This review is limited to remotely viewed comet plasma-tail observations, and it does not include the disintegration of the dusty comet tails and the release of cometary plasma from this material [24, 25], or the possible interaction of this dusty comet material with the solar wind [26].

OBSERVATIONS

The SMEI instrument, launched 6 January 2003 into a ~840 km high terminator Sun-synchronous orbit on the Coriolis spacecraft, provided a view of nearly the whole sky each 102-minute orbit, viewing from within 20° of the Sun out to 180°. SMEI, designed as a pathfinder instrument for the US Air Force Space Test Program viewed solar-wind-plasma surface brightness to its specified limit of at least a 3σ detection (about 0.3 S10)[1] of the background solar wind Thomson-scattering brightness, at 90° from the Sun-Earth line, in one-degree sky resolution elements [27]. Images from this instrument were hampered at times by particle hits during solar storms and during its passage through the auroral ovals and South Atlantic Anomaly (SAA). In addition, SMEI's orbit lies below a then-unknown component of the aurora [28] that at times produces even further image degradation.

SMEI could view any comet brighter than about 10th magnitude that lay within its field of view. Figure 3 shows a fisheye skymap constructed from individual SMEI image frames with stars and background removed (*e.g.*, [29]); here three comets (C/2001 Q4 (NEAT) and C/2004 T7 (LINEAR), and C/2004 F4 (Bradfield) are observed at the same time. These skymaps frequently showed large tail excursions or "kinks" that were previously unobserved (Figure 4; [30, 22]). Buffington et al. [22], measure the radial

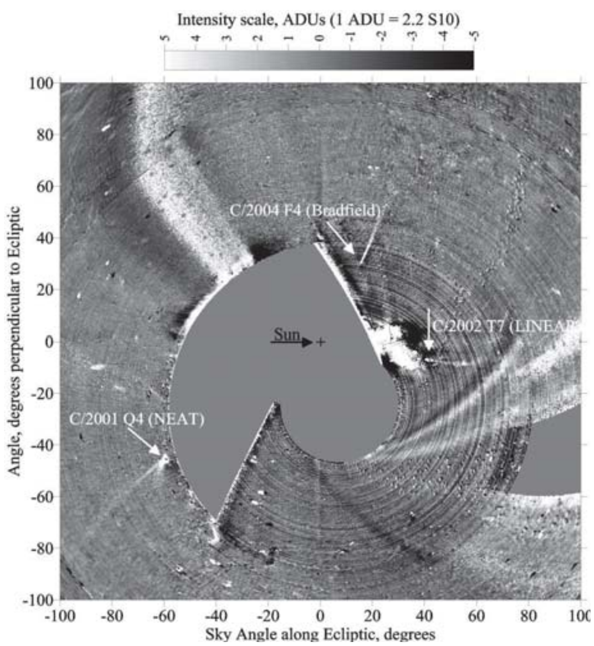

FIGURE 3. Equal-radius fisheye sky map in Sun-centered ecliptic coordinates for an orbit starting at 11:48 UT on 07 May 2004. In this projection, radial angles are mapped linearly from the Sun, and angles around the Sun are preserved over the entire radial distance. Three comets are viewed on this image.

[1] One S10 is the equivalent of one tenth magnitude solar-type star brightness spread over one square degree of sky, or ~2 × 10^{-15} of the solar brightness spread over this same area.

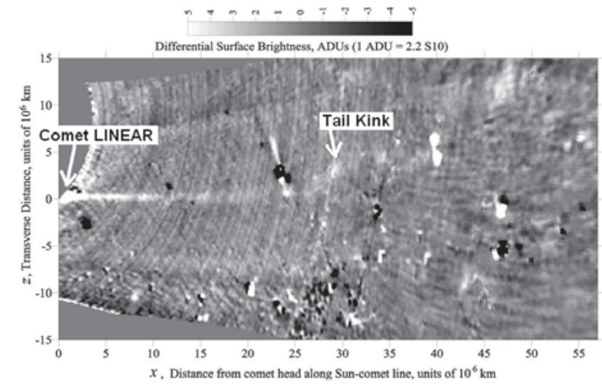

FIGURE 4. View of the tail of comet LINEAR for the SMEI orbit beginning at 02:54UT on 20 May 2004. This represents a single frame in the comet movie. Here the comet nucleus is located at the origin, as shown centered on the left-hand axis. The radial line from the Sun is a horizontal beginning at (0,0).

speed of the plasma tails of comets C/2001 Q4 (NEAT) and C/2004 T7 (LINEAR).

To provide this measurement, Ephemerides obtained from the Minor Planet & Comet Ephemeris Service[2] locate the comet nucleus in 3D space. A straight line from the Sun to the nucleus is projected onto the Sun-centered fisheye skymap as viewed from Earth as for comet NEAT (Figure 5). This original projected line remains fixed in space and time as the sequence of SMEI images steps forward in time and the comet moves in its orbit, providing a new radial (see Figure 6). Features of the comet plasma tail seen in later images, and appearing to cross the earlier radial line are measured and their elongation versus time determined. The elongation is then converted into a radial distance along the Sun-comet line from the temporal and spatial location of the comet nucleus at the time when the line is first projected. The radial distance difference from the nucleus at the time the comet was first observed to the location of the comet tail at this later time gives the radial distance traveled by the plasma, and distance from the nucleus divided by elapsed time provides a radial speed of the solar wind (in this case 0.0808 AU and 283 km s^{-1}, respectively). This process is repeated for each SMEI skymap where sufficient data are available. For each measurement, this indicates the solar wind speed past the comet nucleus assuming no further speed change between the nucleus and the measurement location. Figure 7 shows these speed measurements as a contour plot with the position of the comet nucleus along its orbital path (horizontal axis) versus distance down the Sun-comet line (vertical axis); both are in units of 10^6 km. The dots are the measurement locations along

[2] http://www.cfa.harvard.edu/iau/MPEph/MPEph.html

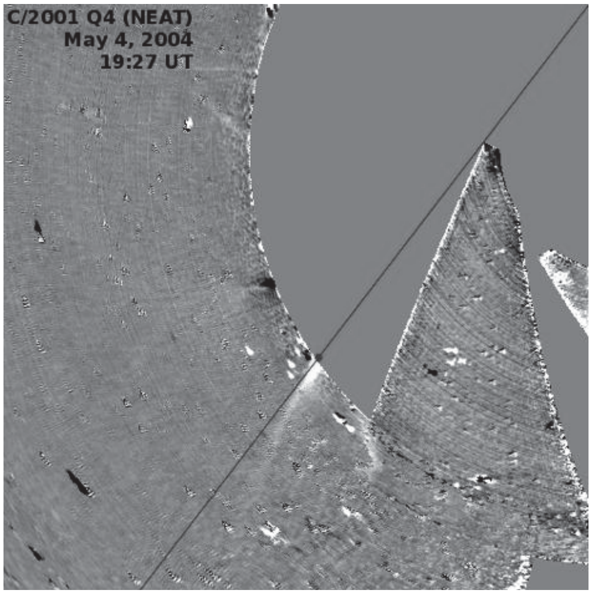

FIGURE 5. A view of Comet NEAT from a 50°×50° section of a SMEI fisheye skymap for the orbit beginning at 19:27 UT on 04 May 2004. The radial from the Sun at the time of the nucleus observation is indicated by a line; the comet nucleus is located at the position of the dot on this line.

each projected radial line. The large low-velocity region at 2.5×10^6 km on the horizontal axis in Figure 7 coincides with the onset of a large "kink" in the plasma tail of the comet (see Figure 6). This low-velocity feature is believed to be related to a solar wind transient observed in the SMEI data [30].

Large speed variations are observed in the radial solar wind determination with slow speeds indicated for the comet at the location of the kink onset. A much higher solar wind speed follows the kink onset a few hours later and after a short travel distance of the comet nucleus. In the cases shown in Figures 5 through 7, the slow speed at the center of Figure 7 begins when the nucleus has moved to 2.7×10^6 km from its onset location on the 19:27 UT 04 May 2004 SMEI image radial shown in Figure 5. The speed of the solar wind increases from a low value of less than 300 km s^{-1} to a speed of over 500 km s^{-1} within a nucleus travel distance of $\sim 1 \times 10^6$ km (0.007 AU) along its orbit. Although these are some of the largest speed variations measured for Comet NEAT by this technique, Figure 7 shows a whole range of speed variations within a span of one and a half days motion of the comet NEAT nucleus.

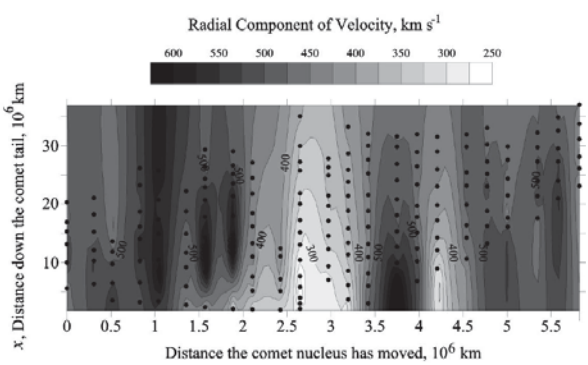

FIGURE 7. NEAT radial velocity contour, beginning at 02:31 UT 4 May through 15:46 UT 05 May 2004 using measurements from SMEI skymaps (from [22]).

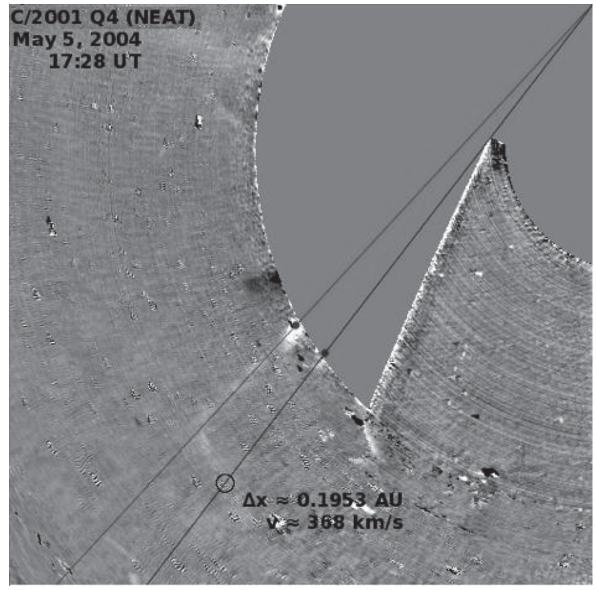

FIGURE 6. A view of Comet NEAT from the SMEI orbit beginning at 07:18 UT on 05 May 2004. The radial from the Sun at the time the SMEI field of view passes the comet nucleus is indicated by a line; the nucleus is located at the position of the dot on this line. A second line with a circle and a dot is the location of the original radial of Figure 5; the circle shows the new comet tail location on this earlier-time radial.

These results are not confined to a single comet. Figure 8 shows a second example of a radial velocity contour plot and average radial solar wind velocity obtained from the STEREO HI-1A images of Comet 96P/Machholz. During this time the comet passed through perihelion at 0.15 AU, and explores the solar wind speed and its variations over a much larger range of solar latitudes and orbit travel distances than the comets viewed by SMEI. In these analyses Machholz travels from a fairly high south latitude (-27°) to a lower latitude (-14°) and from a region of relatively high speed polar solar wind into a region of relatively slow speed wind near the solar equator. Other examples from SMEI and HI-1A images are shown [22, 23] from additional measurements of these same comet plasma tails, and from other comets.

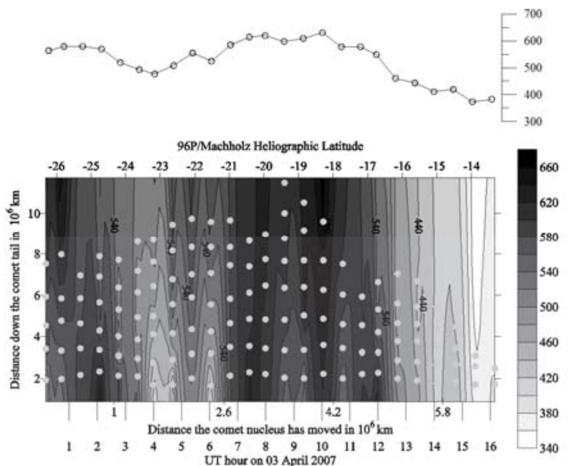

FIGURE 8. *Top:* The average speed in km s^{-1} of each series of radial measurements. *Bottom:* Machholz radial velocity contour, beginning 03 April 2007 at 00:10 UT using measurements from HI-1A images (from [22]).

SUMMARY AND DISCUSSION

Comet plasma tail motions and the ability to trace these motions over large solar distances using spacecraft remote-sensing observations show solar wind motions in a very graphic fashion. These same velocity excursions are measured *e.g.*, by *in-situ* velocity measurements from the Advance Composition Explorer (ACE) [31] spacecraft at 1 AU (Figure 9). In these *in-situ* measurements, the spectral break location at a Δv/v value of ~0.06, and the shallower slope of the spectrum at larger values of Δv/v are claimed to be indicative of the break from a turbulent regime to one where individual structures dominate the solar wind separated by magnetic boundaries [32]. The structures associated with the largest values of Δv/v are known solar wind transients during Coronal Mass Ejections (CMEs) ([30, 33], and see Figure 7), and at the onset of high speed wind streams. The smaller background features that are more numerous in these remotely-sensed comet data of Figure 7 and 8 are more likely the background solar wind structure variations observed as velocity shears between smaller individual magnetic structures as envisioned also by Borovsky [32]. Clearly, the comet plasma-tail measurements only give an indication of the largest solar wind structures present. With these various solar wind structures and studies unknown at the time when many of the initial comet-tail aberration measurements became available (*e.g.*, [4]), it is no wonder that many of these early comet plasma-tail studies give questionable results.

Although the larger-scale solar wind speed structures bounded by the magnetic field flux tubes structures may not be a surprise to some, spacecraft images of comet plasma tails enable a visualization of this as never-before possible. These measurements also provide a precise study of these effects in regions of the heliosphere not yet accessed by direct spacecraft *in-situ* measurements. If comet plasma tails present this effect, so presumably will all other trailing tracers following planetary bodies, such as the field and ions of the Earth's magnetosphere [34].

Currently, other remotely-sensed measurements of these effects are available. In these it is pretty clear that these large velocity shears not directly associated with CMEs may be even more pronounced all the way down to the solar surface, especially in the open magnetic field regions around the Sun. These include observations indicated by multiple and crossing J-map features in enhanced STEREO HI-2 and HI-1 images [*e.g.*, 35, and references therein] that could be different speeds rather than different line of sight structure measurements, and coronal observations near the solar surface where the steep radial coronal gradients restrict LOS measurements to features more nearly in the same plane. These coronal velocity observations are mapped and measured by coronal observations and can be observed in coronal spectrometric data (*e.g.*, [36]) using Solar Ultraviolet Measurements of Emitted Radiation (SUMER) [37] data, and by the Coronal Multi-channel Polarimeter (CoMP) instrument [38], and also from LASCO coronagraph analyses [39]. In these latter analyses, especially in solar polar regions during quiet times when there are no CMEs, the largest solar velocity structures (Figure 10) look very similar to comet plasma-tail observations viewed at far greater distances from the Sun. Some of the linear,

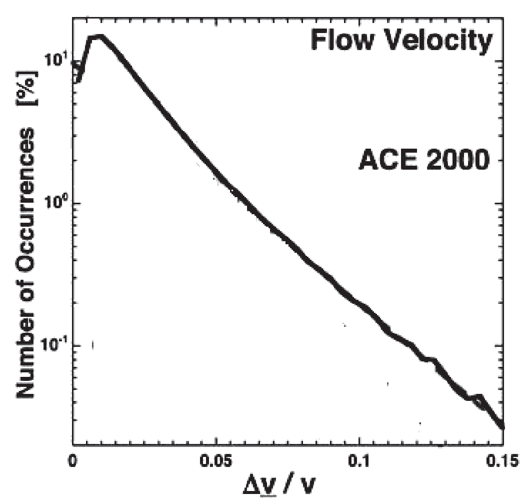

FIGURE 9. Spectrum of solar wind variations from ACE observations during the year 2000 using 64 s velocity observations. At the Δv/v value of ~0.06 there is a break in the spectral properties of the distribution (adapted from [32]).

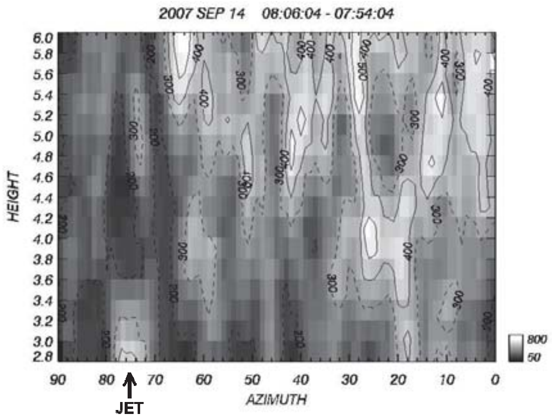

FIGURE 10. Coronal velocity structures measured in the LASCO C2 coronagraph observations by cross correlating consecutive sequential white light images over different heights (see [39]). The analyses map coronal velocity structures at heights from 2.8 to 6.0 Rs in consecutive images from the ecliptic plane (90°) to the ecliptic pole (0°). A jet response is marked.

radial high speed features in these analyses are associated with polar plumes and the onsets of the largest polar jets, and thus have known LOS locations.

In summary, these fine new space-based remote-sensing observations of comet plasma tails provide an application and certification of solar wind variability and some of the new ideas about this variability that are shown by coronal remote-sensing and *in-situ* analyses. These plasma-tail analyses are applicable in the inner heliosphere in regions that are not yet accessible to *in-situ* spacecraft measurements.

ACKNOWLEDGMENTS

The SMEI data analysis presented in these studies was processed at UCSD. SMEI was designed and constructed by a team of scientists and engineers from the US Air Force Research Laboratory, the University of California at San Diego, Boston College, Boston University, and the University of Birmingham, UK. H.-S. Yu, B.V. Jackson, J.M. Clover and A. Buffington were supported at UCSD by NSF grants ATM-0852246, and AGS-1053766, NASA grant NNX11AB50G and by AFOSR grant FA9550-11-1-0324. M.M. Bisi is currently supported by a STFC Standard Grant to Aberystwyth University, Wales, UK. We are also grateful to the LASCO coronagraph group for providing the LASCO C2 and SECCHI H2 images used in this study.

REFERENCES

1. L. Biermann, *Z. Astrophys*., **29**, 274-286 (1951).
2. M. Belton and J. C. Brandt, *Astrophys. J., Suppl*., **13**, 125-332 (1966).
3. E. N. Parker, *Astrophys. J*., **128**, 664-676 (1958).
4. J. C. Brandt, *ARA&A*, **6**, 267-286, (1968).
5. R. Schwenn, in *Phys. of the Inner Heliosphere I*, Springer-Verlag, New York, pp. 99-181 (1990).
6. J. C. Brandt, *et al*., *Astrophys. J*., **196**, 877-878 (1975).
7. A. J. Hundhausen, in *Coronal Holes and High Speed Wind Streams*, J. B. Zirker, ed, pp.225-329 (1977).
8. A. Hewish, *et al., Nature*, **203**, 1214-1217 (1964).
9. W. A. Coles, *et al., Nature*, **286**, 239-241 (1980).
10. J. L. Phillips, *et al*., *Geophys. Res. Letts*, **21**, 01105 doi: 10.1029/94GL01065 (1994).
11. D. J. McComas, *et al., J. Geophys. Res*., **105(A5)**, 10419-10433 (2000).
12. D. J. McComas, *et al., J. Geophys. Res. Letts.,* **30**, 1517-1520 (2003).
13. G. E. Brueckner*, et al.*, *Solar Physics* **162**, 357-402 (1995).
14. D. G. Socker, *et al., Proc. SPIE*, **4139**, 284-293 (2000).
15. R. A. Howard, *et al., Proc. SPIE*, **4139**, 259-283 (2000).
16. R. A. Howard*, et al.*, *Space Science Reviews* **136**, 67-115 (2008).
17. M. L. Kaiser, *Adv. Space Res*., **36**, 1483-1488 (2005).
18. M. L. Kaiser, *et al., Space Sci. Revs*., **136**, 5-16 (2008).
19. C. J. Eyles, *et al*., *Solar Physics* **217**, 319-347 (2003).
20. B. V. Jackson*, et al.*, *Solar Physics* **225**, 177-207 (2004)
21. J. M. Clover, *et al*., presentation at the Second Remote-Sensing Workshop, Aberystwyth, Wales, 6-10 June (2011).
22. A. Buffington, *et al*., *Astrophys. J*., **677**, 798-807 (2008).
23. J. M. Clover, *et al*., *Astrophys. J*., **713**, 394-397 (2010).
24. W. T. Thompson, *ICARUS*, **200(2)**, 351-357 (2009).
25. B. V. Jackson, *et al*., *Ann. Geophys*. **27**, 4097-4104 (2009).
26. C. T. Russell, *et al.,Geophys. Res. Letts*, **36**, 07105 doi:10.1029/2009GL037615 (2009).
27. A. Buffington, *et al*., *Proc. SPIE,* **6689**, 66890B-1 (2007).
28. D. R. Mizuno, *et al., J. Geophys. Res*. **110(A7)**, A07230 (2005).
29. P. P. Hick, *et al., 2007, Proc. SPIE*, **6689**, 66890C-1 (2007).
30. T. A. Kuchar, *et al., J. Geophys. Res*., **113**, A04101 doi:10.1029/2007JA012603 (2008).
31. E. C. Stone, *et al., Space Sci. Revs*., **86**, 1-22, (1998).
32. J. E. Borovsky, *J. Geophys. Res*., **113**, A08110, doi:1029/2007JA012684 (2008).
33. A. Vourlidas, *et al., Astrophys. J*., **668**, L79-L82 (2007).
34. J. E. Borovsky, *J. Geophys. Res*., **117**, A06224 doi:10.1029/2012JA017623 (2012).
35. DeForest, *et al*., *Astrophys. J.* **738**:103, doi:10.1088/0004-637X/738/1/10 (2011).
36. S. W. McIntosh and B. De Pointieu, *Astrophys. J*., **707**, 524-538 (2009).
37. K. Wilhelm, *et al*., *Solar Phys.* **162**, 189-231 (1995).
38. S. W. McIntosh, *et al*., *SHINE Conference Proc.*, 25-29 June (2012).
39. H. -S. Yu, *et al*., in *AIP Conf. Proc. - Solar Wind Thirteen* (this issue) (2012).